Comprehensive Analysis of Tumor Immune Microenvironment and Prognosis of m6A-Related lncRNAs in Gastric Cancer

Yi Wang
Department of Radiology, Zhongshan hospital
Gui-Qi Zhu
Liver Cancer Institute, Fudan University
Di Tian
Department of Radiology, Zhongshan hospital
Chang-Wu Zhou
Department of Radiology, Zhongshan hospital
Na Li
Department of Radiology, Zhongshan hospital
Ying Feng
Affiliated Hospital of Nantong University
Meng-Su Zeng (zhudahuaidan@yeah.net)
Department of Radiology, Zhongshan hospital

Research Article

Keywords: N6-methyladenosine, long non-coding RNAs, tumor immune microenvironment, prognosis, immune checkpoints inhibitors therapy, gastric cancer

Posted Date: June 2nd, 2021

DOI: https://doi.org/10.21203/rs.3.rs-558845/v1

Version of Record: A version of this preprint was published at BMC Cancer on March 24th, 2022. See the published version at https://doi.org/10.1186/s12885-022-09377-8.

Title page

Title

Comprehensive analysis of tumor immune microenvironment and prognosis of m6A-related lncRNAs in gastric cancer

Running head: M6A-related lncRNAs in gastric cancer

Authors' name

Yi Wang[1#], Gui-Qi Zhu[2#], Di Tian[1], Chang-Wu Zhou[1], Na Li[1], Ying Feng[3]**, Meng-Su Zeng[1]**

Institution

[1]Department of Radiology, Zhongshan Hospital, Fudan University, Shanghai Institute of Medical Imaging, Xuhui District, Shanghai, 200032, China.

[2]Department of Liver Surgery and Transplantation, Liver Cancer Institute, Zhongshan Hospital, Fudan University, Shanghai, 200032, China

[3]Department of Gastrointestinal Surgery, Affiliated Hospital of Nantong University, 20 Xisi Street, Nantong, Jiangsu, 226000, China

****Correspondence:** Meng-Su Zeng, MD, PhD

200032, 200032, China.

E-mail: zhudahuaidan@yeah.net

Ying Feng, MD, PhD

Department of Gastrointestinal Surgery, Affiliated Hospital of Nantong University, 20 Xisi Street, Nantong, Jiangsu, 226000, China

E-mail: fengying7017@163.com;

[#] These authors contributed to this work equally.

Abstract

Background

N6-methyladenosine (m6A) modification and long non-coding RNAs (lncRNAs) play pivotal role in gastric cancer (GC) progression. The emergence of immunotherapy in GC has created a paradigm shift in the approach of treatment, whereas there is significant heterogeneity with regard to degree of treatment responses, which results from the variability of tumor immune microenvironment (TIME). How the interplay between them enrolled in the shaping of TIME remains unclear.

Methods

The RNA sequencing and clinical data of GC patients were collected from TCGA database. Pearson correlation test and univariate Cox analysis were used to screen out m6A-related lncRNAs. Consensus clustering was implemented to classify GC patients into 2 subtypes. Survival analysis, the infiltration of immune cells, Gene set enrichment analysis (GSEA) and the mutation profiles were analyzed and compared between two clusters. Then least absolute shrinkage and selection operator (LASSO) COX regression was implemented to select pivotal genes and risk score model was constructed accordingly. The prognosis value of the risk model was explored. In addition, the discrepancies of response to immune checkpoints inhibitor (ICIs) therapy were compared between different risk groups. Finally, we performed qRT-PCR to detect the expression pattern in 35 tumor tissues and paired adjacent normal tissue, and validated the prognostic value of risk model in the our cohort (N=35).

Results

The expression profiles of 23 lncRNAs were included to cluster patients into different subtypes.

Cluster1 with worse prognosis harbored higher immune score, stromal score, ESTIMATE score and mutation rate of genes. Different immune cell infiltration pattern were also displayed between different clusters. GSEA showed that cluster1 was preferentially enriched with tumor hallmarks and tumor correlated biological pathways. Next, 9 lncRNAs were selected by LASSO regression model to construct risk model. Patients in the high risk group had poor prognosis. The prognosis value of this model was also validated in our cohort. As for predicting responses to the ICIs therapy, we found that patients from high risk group had lower TMB score and lower proportion of MSI-H subtype. Moreover, patients had distinct immunophenoscores in different risk groups.

Conclusion

Our study revealed that the potential interplay between m6A modification and lncRNAs might have critical role in predicting GC prognosis, sculpting TIME landscape and predicting the responses to immune checkpoints inhibitors therapy.

Keywords: N6-methyladenosine, long non-coding RNAs, tumor immune microenvironment, prognosis, immune checkpoints inhibitors therapy, gastric cancer

Introduction

Gastric cancer (GC) is the fifth most lethal tumor and estimated to be the third most common cause of cancer-related death (1, 2). Accumulating researches have suggested that epigenomic alterations acted as a crucial role through activation of oncogenes or tumor suppressor genes in the gastric carcinogenesis (3, 4). Presently, N6-methyladenosine (m6A) is the most common RNA modifications, which was discovered not only in mRNAs, but also in ncRNAs, such as

microRNAs (miRNAs), long non-coding RNAs (lncRNAs) and circular RNAs (circRNAs) through modulating the splicing, stability and translation of ncRNAs (5). Intriguingly, noncoding RNAs were also demonstrated to have regulatory role for the expression of m6A regulatory proteins. Therefore, the interaction between m6A and noncoding RNAs exerts a synergistic effect on carcinogenesis and provides novel cancer treatment strategies (6-8). To note, according to the previous researches, the interplay models between m6A modification and lncRNAs in tumor were diverse and complex. For instance, miR503HG promoted the degradation of HNRNPA2B to inhibit HCC migration via reducing the stability of p52 and p65 mRNA (9). GATA3-AS acted as a guide lncRNA which promoted the m6A modification of GATA3 pre-mRNA by KIAA 1429, thereby down-regulating the expression of GATA3, and contributed to the growth and the metastasis of HCC(10), LINC00470 interacted with METTL3 in GC leading the suppression of the stability of PTEN which is demonstrated as a tumor suppressor (11). Recently, with the increased understanding of the diversity of tumor microenvironment (TME), cross-talk between tumor cells and the surrounding cells plays a crucial role in the tumor progression (12). Meanwhile, m6A modification was reported to be critically associated with tumor microenvironment immune pattern and PD-L1 expression in gastric cancer, colon cancer and head and neck squamous cell carcinoma (13-15), from these above studies, it could be referred that m6A modification served as a powerful predictor for recruiting candidates for immune checkpoint blockade immunotherapy. Another study showed that a nine m6A-related lncRNAs based prognostic model could forecast the 5-year overall survival (OS) of patients with lower-grade glioma with the C-index of 0.781 (16). However, the underlying regulatory biological process between m6A and lncRNAs in GC, especially their clinical applications in predicting prognosis

and immunotherapeutic effects remains elusive.

In the present study, we attempted to comprehensively evaluate the correlations of m6A-related lncRNAs with prognosis, immune cell infiltrating and response to immune checkpoints inhibitors in GC patients. These associations were analyzed multidimensionally, patients with GC were firstly clustered into distinct subtypes characterized by different expression patterns of m6A-related lncRNAs, and then they were also categorized into high risk and low risk groups by the construction of prognostic model. The interrelationship of the two types of stratification were further evaluated to confirm that the model based on m6A-related lncRNAs as a robust prognostic biomarker for GC. Moreover, our study revealed that m6A-related lncRNAs played a nonnegligible role in shaping tumor immunity features and predicting responses to immune checkpoints inhibitors, which could shed light on the mechanism of the correlation of m6A modification with immunology and provide insights into the immunotherapy in GC.

Materials and Methods

Data collection and processing

RNA sequencing data and clinical information were downloaded from the TCGA database via the GDC data portal (https://portal.gdc.cancer.gov/repository) and the raw count data of 375 GC samples and 32 normal samples were collected. Next, we obtained a total of 14086 lncRNAs according to the Ensemble IDs of the genes for further analysis. Additionally, corresponding clinical information of patients with GC was also collected. Patients with missing status or time information of over survival (OS) were excluded. Ultimately, 371 GC patients with lncRNA expression data and clinicopathological information including age, gender, grade, stage and TNM

staging were selected in the final cohort for analysis. A total of 371 patients were randomly assigned into the training or validation cohort at the ratio of 7:3 using the caret package. The baseline characteristics of the included TCGA-STAD dataset were summarized in Table 1. Continuous variables were converted to categorical variables for further analysis, variables in the training and validation cohort were compared using the chi-square test. To acquire of somatic mutation data, we downloaded "Masked Somatic Mutation" data and used VarScan software to process it. We implemented "maftools" to analyze and visualize the Mutation Annotation Format (MAF) of somatic variants. Microsatellite instability status (MSI) and immunophenoscore information (IPS) for each sample in TCGA-STAD were downloaded from The Cancer Immunome Database (TCIA) (https://tcia.at/home).

Identification of m6A-related genes and prognostic m6A-related lncRNAs

Based on previous publications, expression matrixes of 23 m6A-Related genes were extracted according to the mRNA expression data in TCGA-STAD, including expression data on writers (METTL3, METTL14, METTL16, WTAP, VIRMA, ZC3H13, RBM15 and RBM15B), readers (YTHDC1, YTHDC2, YTHDF1, YTHDF2, YTHDF3, HNRNPC, FMR1, LRPPRC, HNRNPA2B1, IGFBP1, IGFBP2, IGFBP3 and RBMX) and erasers (FTO and ALKBH5). Subsequently, m6A-related lncRNAs were first filtered using the "limma" R package by setting cor > 0.5 and p value < 0.05 and co-expression network graph was plotted by the "igraph" R package. Then univariate Cox regression analysis was conducted to screen the prognostic m6A-related lncRNAs with the criterion of p value < 0.05. Wilcoxon test was applied to examine the expression differences of lncRNAs between GC tissue and normal adjacent tissues.

Identification of m6A-related lncRNAs subgroups by consensus clustering

To further explore the underlying biological characteristics of the m6A-related lncRNAs, patients with GC were clustered into different subtypes using the "ConsensusClusterPlus" R package with iterations of 50 and resample rate of 0.8. The optimal k value (k=2) was determined to obtain a stable cluster. Kaplan Meier survival method and log rank test were used for subgroup analysis of clinicopathological factors between two clusters.

Analysis of the correlations of different clusters with TIME.

Scores of immune, stromal and ESTIMATE were calculated using ESTIMATE algorithm by the "estimate" package. Expression differences of immune, stromal and ESTIMATE score between the two clusters were analyzed by wilcoxon test. CIBERSORT algorithm was used to evaluate the fraction of 22 immune cell types for each sample. We conducted Wilcoxon test to compare the abundance of immune infiltrating cells between two clusters.

GSEA was conducted to investigate the differences in tumor signaling pathways of patients in cluster1 compared with those in cluster2 with random sampling of 1,000 permutations, setting the false discovery rate (FDR) < 0.05 as the cut-off value.

Construction and validation of the risk model and its association with clinicopathological features and immune infiltrating cells

The least absolute shrinkage and selection operator (LASSO) regression algorithm was implemented to further select the m6A-related lncRNAs most associated with overall survival in

the training cohort using the “glmnet” package. Thereafter, the expression level of the 9 identified lncRNAs and corresponding coefficients obtained from the LASSO regression algorithm were used to establish the risk model, the following risk score formula is present: Risk score = coef1*x1+coef2*x2+coef3*x3+...+coefi*xi (coef refers to the coefficient of each lncRNA and x refers to the expression level of each lncRNA). Patients were divided into high risk and low risk group in both training and testing group according to the median risk score. To evaluate the predictive accuracy of the risk model, receiver operating characteristic (ROC) was applied in training and validation cohorts. Kaplan Meier survival method and log rank test were implemented to detect the OS difference between low risk and high risk group. Subsequently, subgroup analysis stratified by clinicopathological features was utilized in different risk group. Univariate and multivariate Cox regression analysis were conducted to evaluate whether the risk score was independent prognostic factor. Wilcoxon test was implemented to further explore the risk score differences with regard to clinicopathological factors, immune score, TMB scores, IPS and two clusters. Pearson correlation test was implemented to evaluate the relationships of risk scores with the abundance of immune infiltrating cells and TMB scores.

Calculation of TMB scores

We calculated the mutation frequency with number of variants/the length of exons (38 million) for each sample via Perl scripts based on the JAVA platform. Wilcox test and Pearson correlation analysis were conducted to analyze the relationship between TMB and risk score.

External validation in clinical samples

We collected tumor samples and adjacent normal samples from 35 GC patients with surgical resection from the Affiliated Hospital of Nantong University. The baseline information of 35 patients were showed in Table 1. Fresh tumor and adjacent normal tissue were stored at -80℃. This research was approved by the Clinical Research Ethics Committee of the Affiliated Hospital of Nantong University (2021-L018). For evaluating the expression levels of the selected 9 m6A-related lncRNAs, total RNA from 35 gastric cancer samples and their adjacent normal tissues were extracted by using MolPure Cell RNA Kit (YEASEN Biotech Co., Ltd). cDNA synthesis was carried out by using Hifair III 1st Strand cDNA Synthesis SuperMix for qPCR (YEASEN Biotech Co., Ltd). The relative lncRNA expression levels were calculated with $2^{-\Delta\Delta CT}$ method, GAPDH was served as an internal control, the sequences of qPCR primers were presented at Table S1. Risk score was calculated by the above constructed formula, median risk score was determined as the cut-off value. Then univariate and multivariate Cox regression analysis, Kaplan Meier analysis, time-dependent ROC curve and calibration curve were conducted for the validation of prognosis value in the external cohort (N=35).

Results

Identification of m6-related lncRNAs in GC patients

The study flowchart is shown in Figure 1. A total of 14086 lncRNAs and expression matrixes of 23 m6A-related genes were extracted from TCGA-STAD RNA sequencing dataset. The value of pearson correlation > 0.5 and p value < 0.01 were set as the criterion for preliminarily selecting m6A-related lncRNAs. 491 lncRNAs were found to be significantly correlated with m6A-related

genes. The co-expression network graph was shown in Figure 2A. Subsequently, 23 lncRNAs were obtained by univariate Cox regression analysis ($P<0.05$) when the prognostic information was integrated. The forest plot showed that 11 of the screened lncRNAs were risk factors with HR (Hazard ratio) > 1 and others are protective factors with HR (Hazard ratio) < 1 (Figure 2B). The heatmap (Figure 2C) and the boxplot (Figure 2D) demonstrated that the 23 lncRNAs expression pattern in the GC tissues compared with those in the normal tissues (Figure 2C and 2D).

Consensus clustering identified two clusters of GC with distinct prognoses based on m6A-related lncRNAs

Based on the similarity of the expression of the 23 lncRNAs in GC samples, Consensus Clustering Method was applied to cluster the samples to further elucidate the biological discrepancies among subgroups. The CDF curves of consensus matrix indicated that when k=2, the interference between subgroups is minimal and the distinction is significant (Figure 3A-C). A total of 371 GC patients were separated into cluster1 (n=266) and cluster2 (n=105). As illustrated in the survival plots, patients in cluster1 subgroup had worse OS than their cluster2 counterparts. (Figure 3D).

The association of the two clusters and GC patients' prognosis was further indicated by comparing survival rates of the two clusters in different clinical subgroups. The survival plots were drawn (Figure 3E-I) and the results showed that survival rates of 2 clusters had significant differences in age <= 65 ($p<0.001$), male ($p=0.018$), female ($p=0.044$), grade3 ($p=0.01$), stage III + stage IV ($p=0.007$).

Tumor immune microenvironment (TIME) and mutation profile of two clusters

To get deeper insights into the interplay between m6A-related lncRNAs and immunity, TIME as a crucial cellular milieu for immune cells, stromal cells and extracellular matrix molecules has predominant impact on the tumor progression, hence, the distribution differences of the estimated proportion of immune and stromal between the 2 clusters were calculated by ESTIMATE algorithm. As shown in Figure 4A-C, cluster1 harbored higher immune score ($p<0.001$), stromal score ($p<0.001$) and ESTIMATE score ($p<0.001$). These findings revealed that larger amount of immune and stromal components in TIME of GC were associated with worse survival outcome. To elucidate the specific immune cells distribution pattern in two subtypes, the fraction of 22 immune cell types was analyzed (Figure 5G) and we discovered that cluster1 was enriched in CD4 memory resting T cells ($p<0.001$) (Figure 5B), monocytes ($p=0.0096$) (Figure 5D) and resting mast cells ($p<0.001$) (Figure 5F). Conversely, cluster2 was enriched in CD4 memory activated T cells ($p<0.001$) (Figure 5A), follicular helper T cells ($p<0.001$) (Figure 5C) and M1 macrophages ($p=0.021$) (Figure 5E).

For investigating the biological mechanism of contributing the heterogeneity of the two clusters, GSEA was implemented and we found that several tumor hallmarks were dynamically enriched in the cluster1 compared with cluster2, including cell adhesion molecules (normalized enrichment score [NES]=2.03, normalized $p=0.004$), ECM receptor interaction (NES=2.18, normalized $p<0.001$), focal adhesion (NES=2.11, normalized $p<0.001$) (Figure 4D-F). Aforementioned multiple signaling differences between the two clusters indicated the potential role of m6A-related lncRNAs in gastric carcinogenesis.

Finally, we evaluated the association between mutation profiles and two clusters. The mutation profiles of each sample in 2 clusters (cluster1: 93.85%, cluster2: 82.97%) were presented

respectively (Figure 6A, B). We found the discrepancy of the proportion of mutated genes with substantial different frequencies in two clusters, providing insights into the m6A-related lncRNAs regulatory network in gastric cancer.

Construction and validation of a prognostic model for GC patients based on m6A-related lncRNAs

As assessed by the univariate Cox regression analysis, 23 differentially expressed m6A-related lncRNAs were found significantly associated with OS. To identify the most powerful prognostic m6A-related lncRNAs, LASSO regression analysis was performed, and nine lncRNAs containing AC026691.1, AL139147.1, AL590705.3, AC022031.2, TYMSOS, AL355574.1, AL390961.2, AC005586.1 and AP000873.4, and coefficient of each lncRNAs were finally identified (Figure 7A-C). Based on the regression coefficients and expression values of the 9 prognostic markers, a risk model was constructed, and the following formula was present: risk score = 0.4785 * expression (AC026691.1) + 0.4706 * expression (AL139147.1) + 0.3874 * expression (AL590705.3) + 0.1807 * expression (AC022031.2) - 0.0586 * expression (TYMSO) - 0.1085 * expression (AL355574.1) - 0.2289 * expression (AL390961.2) - 0.2734 * expression (AC005586.1) - 0.3635 * expression (AP000873.4). According to the median value of the risk score. GC patients were divided into high risk group and low risk group. The survival analysis were conducted in different risk groups and showed that both in training cohort or validation cohort, GC patients from high risk group had worse survival outcome ($P<0.001$) (Figure 7D, 7E) The ROC curves were utilized to evaluate the predictive performance of risk model, and the area under the ROC curve (AUC) for OS was 0.705 in the training cohort (Figure 7F) and 0.682

(Figure 7G) in the validation cohort. Moreover, the distribution of risk scores and survival status of each patient in the both training and validation cohort were displayed in Figure 7H and Figure 7I. These figures indicated that with the increase of the risk score, the mortality rate was increased and the survival time was shorter. The heatmap indicated that distinct expression pattern of the 9 lncRNAs between different risk group. Taken together, our results suggested that the risk scores based on the 9 m6A-related lncRNAs had optimal predictive ability of the prognosis of GC patients.

Risk score based on the m6A-related lncRNAs was an independent prognostic factor for GC patients

In the subgroup analysis for GC patients with different risk groups from age, gender, grade and stage subgroup, all p values were less than 0.001 calculated by log rank analysis (Figure S1). Then we performed univariate and multivariate Cox regression analysis to determine whether the risk model based on the m6A-related lncRNAs could independently predict the prognosis of GC patients. The results of univariate Cox regression analysis showed that OS was evidently associated with age (HR, 1.028; 95%CI, 1.004-1.054, p=0.024) and risk score (HR, 10.409; 95%CI, 5.025-21.564, p<0.001) in the training cohort, and significantly associated with stage (HR, 1.879; 95%CI, 1.351-2.614, p<0.001) and risk score (HR, 4.490; 95%CI, 1.823-11.061, p=0.001) in the validation cohort. After adjusting the clinicopathological factors such as age, gender, grade and stage in the multivariate Cox regression analysis, age (HR, 1.035; 95%CI, 1.009-1.062, p=0.009), stage (HR, 1.402; 95%CI, 1.059-1.856, p=0.018) and risk score (HR, 11.097; 95%CI, 4.830-25.493, p<0.001) in the training cohort, and age (HR, 1.037; 95%CI, 1.010-1.064, p=0.007),

stage (HR, 2.023; 95%CI, 1.417-2.887, p<0.001) and risk score (HR, 6.411; 95%CI, 2.394-17.172, p<0.001) in the validation cohort acted as the powerful prognostic factors (Table 2).

Prognostic risk score was associated with clinicopathological factors and immune infiltrating cells

First off, we further evaluated the relationship between risk and the 9 prognostic m6A-related lncRNAs. As expected, it could be concluded from the heatmap that all the 9 prognostic m6A-related lncRNAs had relatively different expression values in patients from two risk groups (Figure 8A). Next, it can be also referred from the heatmap and the scatter diagrams (Figure 8B-E) that statistical difference of risk score existed in the stratification of cluster (p<0.001), stage I-II vs stage III-IV (p=0.012), grade1+grade2 vs grade3 (p<0.001), N0 vs N1-3 (p=0.03). Moreover, the relationship between risk score and immune infiltrating cells abundance was explored, we found that CD4 memory activated T cells, macrophages M0, follicular helper T cells and memory B cells were negatively associated with risk score, while macrophages M2 and resting dendritic cells were positively associated with risk score, with all p value less than 0.001 (Figure 9A-F). Collectively, these facts strongly indicated that risk score established on m6A-related lncRNAs exhibits valuable clinical information and had crucial clinical implication value.

Risk score was associated with biomarkers for response to immune checkpoint inhibitors.

We attempted to further excavate the value of the risk model constructed based on 9 m6A-related lncRNAs in predicting patients' immunotherapeutic outcomes. Higher TMB was characterized by favorable responses to immune checkpoint inhibitors. In our study, high TMB was correlated with

lower risk score ($p<0.01$) calculated by Wilcox test (Figure 10A). Risk score was negatively associated with tumor mutation burden (cor = -0.36, $p<0.01$) (Figure 10B). We also analyzed the distribution differences of microsatellite instability subtypes between low and high riskScore group. As presented in Figure 10C, low risk score group showed higher proportion of MSI-H subtype (24% vs 12%) and lower proportion of MSS (62% vs 72%) and MSI-L (14% vs 15%) than that of high riskScore group, on the other hand, MSI-H group exhibited markedly lower risk score than MSI-L group ($p=0.008$) and MSS group ($p<0.001$), however, no distribution differences of risk score were observed in MSS and MSI-L group ($p=0.55$) (Figure 10D). In addition, the relationship between risk score and immunophenoscore which was a predictor of response to anti-cytotoxic T lymphocyte antigen-4 (CTLA-4) and anti-programmed cell death protein 1 (anti-PD-1) were explored. The results showed that low and high risk group tends to have different immune checkpoint inhibitor responses including anti-CTLA-4 therapy, anti-PD-1 therapy or combination of both therapy (Figure 10E-H). Our findings strongly indicated that m6A-related lncRNAs had superior values in optimize candidates' selection for ICI therapy and predicting patients' outcomes of ICI therapy.

External validation of 9 m6A-related lncRNAs based risk model in the clinical dataset.

We collected 35 GC patients from Zhongshan hospital, Fudan university as the external validation cohort. First, we quantitated the relative expression levels of the 9 lncRNAs in 35 tumor tissues and adjacent normal tissues by quantitative RT-PCR, the results demonstrated that the expression pattern of the 9 lncRNAs in our cohort was consistent with TCGA dataset. Four lncRNAs (AC026691.1, AL139147.1, AL590705.3 and AC022031.2) were generally up-regulated in tumor

tissues, while the other five lncRNAs (TYMSOS, AL355574.1, AL390961.2, AC005586.1 and AP000873.4) were mainly down-regulated in tumor tissues (Figure 11A). Based on the expression level of each lncRNA, we calculated the risk score of each patient and divided total cohort into high and low risk group using median risk score as the cutoff value (2.981), and the baseline clinical information of patients from different risk groups were displayed in the Table 3. We found that patients from high risk group had worse OS compared with those from low risk group (p=0.0064) (Figure 11B). Univariate and multivariate cox analysis confirmed that the risk score was an independent prognosis predictor (Table 2). To further identify the prognostic value of the risk model, The ROC of the risk score for predicting OS of the external clinical cohort was 0.835 (Figure 11C). Additionally, time-dependent ROC analysis was applied and the AUC ranges from 0.829 to 0.967 (Figure 11D), demonstrating a satisfactory prognostic value. Finally, the calibration curve for the risk score showed good agreement between prediction and actual OS status (Figure 11E).

Discussion

The interaction pattern between m6A and lncRNAs can be separated into two subtypes. On one hand, m6A modification on lncRNA acts as a structural switch to facilitate RNA-protein interactions. M6A can also mediate the function of lncRNAs by increasing the stability of the transcript of lncRNAs via ceRNA model (7, 17). For instance, HNRNPC can bind to MALAT1, which is a conserved lncRNA whose upregulation was correlated with carcinogenesis, thereby influencing RNA expression and alternative splicing (18). METTL3 mediated m6A modification could stabilize the expression level of LINC00958 that functioned as a competitive endogenous

RNA (ceRNA) to facilitate the progression of HCC (19). On the other hand, lncRNAs could also regulate the m6A regulatory proteins to promote their functions. It was recently reported that in glioblastoma stem-like cells (GSCs), ALKBH5 as a m6A eraser could demethlyse FOXM1 nascent transcripts and enhanced FOXM1 expression. Meanwhile, the FOXM1-AS which was a lncRNA antisense to FOXM1 acted as a promoter for the interaction of ALKBH5 and FOXM1, contributing to the overly expressed FOXM1 and GSC proliferation (20). Similar mechanism was found to lead to cervical cancer mediated by the interaction between ALKBH5 and GAS5-AS1 (21). Collectively, the sophisticated regulatory network between m6A and lncRNAs provides new possibility in exploring the biological features of carcinogenesis and clinical application roles. Therefore, we performed integrated analysis of m6A-related lncRNAs associated with clinical characteristics in GC patients, indicating that two subtypes characterized by distinct expression patterns of lncRNAs had significantly different OS outcome. Besides, the risk score constructed by 9 prognostic m6A-related lncRNAs were also remarkably related with OS outcome, two clusters, Stage and N stage, thus it's not surprising to find that cluster 1 were correlated with high risk group, sharing the consistently poorer prognosis outcome. This demonstrated that the risk model constructed based on m6A-related lncRNAs was a robust and reliable GC clinical indicator. More importantly, the risk score model was satisfactorily validated in the external cohort, which confirmed its prognostic value.

Several studies have revealed that m6A has diverse functions in cancer immunity through different m6A regulators. YTHDF1 depletion in dendritic cells could enhanced the cross-presentation of tumor antigens and cross-priming of CD8+ T cells (22). Besides, colon

cancer with METTL3 or METTL14 deficient increased cytotoxic CD8+ T cells infiltrating in tumor microenvironment (23). In melanoma, FTO could not only promote tumor progression but also leaded to anti-PD1 resistance . Zhang et al (13) identified three distinct m6A modification patterns based on 21 m6A regulators in 1938 GC patients and found that these three patterns were highly associated with different immune phenotypes. Similar findings were also determined in colon cancer (14). LncRNAs are also crucial in mediating the development of diverse immune cells (24). For example, LncRNA UCA1 elevated the expression of PD-L1 via direct interaction with miRNAs in GC (25). The lincRNA NeST functioned as a regulator for Th1 cell differentiation (26). LncRNA FAS-AS1 was known to regulate FAS receptor signaling in B cell lymphomas and elevated level of FAS-AS1 may lead to uncontrolled proliferation of B cells (27). Recently, a new method called ImmLnc pipeline was invented to identify critical lncRNAs involved in immunology and exhibited satisfactory validation outcome in non-small cell lung cancer (28). Together, although there have been many studies indicating the separative biological function of m6A or lncRNA enrolled in the immunity, the integrated analysis of regulatory spectrum of them in TIME is still obscure.

Immunotherapy has revolutionized the oncology landscape, especially the ICI therapy has gained enormous success in multiple solid tumors (29). In advanced GC, inhibition of PD-1/PD-L1 could improve the 18- month OS rate and prolonged the response duration reported by a meta-analysis study (30). However, only a subset of GC patients can benefit from this novel therapy due to the heterogeneity of immune microenvironment (31). Therefore, comprehensive analysis of TIME is mandatory for recruiting patients for ICIs therapy. TIME plays a pivotal role in mediating tumor

progression by inducing epithelial mesenchymal transition (EMT) in the tumor cells. Stromal cells in the surrounding environment are recruited to the area where the tumor cells localize and promote the distant metastasis (12, 32). Previous studies investigated the correlation of immune cells in the TIME with GC prognosis. They found that memory T cells, cytotoxic CD8+ and Natural Killer (NK) cells were associated with better survival outcome (33, 34). It is worth noting that stromal cells secreted growth factors responsible for the activation of Wnt signaling in the nucleus, and Wnt ligands secreted by tumor cells would drive the phenotype of tumor associated macrophage towards M2 subtype which is considered anti-inflammatory via the Wnt signaling pathway, resulting in the tumor progression (35). Consistent with the above descripted tumor-stromal-immune cell cross-talk, we found cluster2 with better prognosis was enriched in M1 subtype which is considered pro-inflammatory, and exhibited less activated status in stromal cells, furthermore, the expression level of M2 subtype was positively correlated with the risk score. It is noteworthy to mention that T cells follicular helper (Tfh) was positively associated with long term survival in GC patients according to our results. As previous work indicated, Tfh cells were supportive for the recruitment of CD8+ T cells, NK cells and marcophages that engage in anti-tumor immunity, and germinal center Tfh cells were reported to express markedly high level of PD1 (36). Moreover, we also found that the risk score was negatively correlated with memory B cells, resting dendritic cells, and macrophage M0, and positively correlated with monocytes. Taken together, we systematically analyzed the complex components of TIME including immune infiltrating cells and stromal cells, finding that the establishment of the risk score and two subtypes based on m6A-related prognostic lncRNAs were significantly correlated with TIME. It suggested that m6A-related lncRNAs are dynamically involved in TIME reprogramming. To

further unveil the potential role of m6A-related lncRNAs in guiding ICI therapy, we investigated the relationship of various biomarkers including TMB, MSI and IPS with our constructed risk model. TMB has evolved as an effective biomarker for recruiting patients who possibly respond to ICI therapy and patients with high TMB could gain better survival outcome from immunotherapy. MSI is a molecular indicator of defective DNA mismatch repair (MMR). MSI-H was correlated with favorable survival outcomes compared with MSS and MSI-L in GC (37) and MSI was demonstrated to be a robust indicator for immune checkpoint blockade therapy in the KEYNOTE studies (38, 39). In our study, patients of low risk had higher TMB and account for larger proportion of MSS-H subtypes, which is consistent with the research conducted by Chalmers (40). Thus, the result suggested that patients in low risk group more likely benefited in ICI therapy.

However, there are several limitations in our study. First, the efficacy of our model needs to be further validated in the external cohort of larger number. Second, since these selected m6A-related lncRNAs have never been reported in GC, the functions of these selected m6A-related lncRNAs should be confirmed further with functional experiments. Finally, the specific regulatory network between m6A and lncRNA, and their interaction role of participating in TIME should be further unveiled.

Conclusion

We conducted an in-depth bioinformatic analysis of the regulatory mechanisms of M6A-related lncRNAs in GC. M6A-related lncRNAs were screened out with integrating prognosis information. Two subtypes of GC (cluster 1 and cluster 2) patients based on different lncRNAs expression

pattern were distinct in TIME characteristics, gene variants and OS outcome. Moreover, prognostic m6A-related lncRNAs based risk score were highly associated with two subtypes, clinicopathological features and immune infiltrating cells. In addition, patients from low risk group are more likely to benefit from ICI therapy. The prognostic value of the risk model was validated in the external clinical cohort. These results provided more mechanisms in GC evolutionary and pave the way for the development of immunotherapy.

Ethics approval and consent to participate

This study protocol which involved human participants was approved by the Clinical Research Ethics Committee of the Affiliated Hospital of Nantong University (2021-L018), and informed consent was obtained from all of the patients. All the data and material have been performed in accordance with the Declaration of Helsinki.

Consent for publication

Not applicable

Availability of data and materials

Publicly available database analyzed in this study can be found in the The Cancer Gernome Altas (https://portal.gdc.cancer.gov/). The dataset of external cohort of our hospital is available from the corresponding author upon reasonable request.

Competing interests

The authors declare no disclosures.

Funding

This work was supported by grants from the National Natural Science Foundation of China (grant number 91859107), the Shanghai Science and Technology Committee (grant number 18DZ1930102, grand number 19411965500), the Shanghai Municipal Key Clinical Specialty (W2019-018), the Clinical Research Plan of SHDC (SHDC2020CR1029B) and Zhongshan Hospital, Fudan University (grant number 2018ZSLC22, 2020ZSLC61).

Authors' contributions

Wang Y, Zhu GQ and Tian D designed the study. Wang Y and Zhu GQ collected clinical data. Wang Y and Zhu GQ did the statistical analyses. Feng Y collected tumor tissues and performed the quantative PCR. Li N prepared figures. Wang Y, Zhu GQ, Li N, Feng Y and Zeng MS reviewed the results, interpreted data and wrote the manuscript. All authors have made an intellectual contribution to the manuscript and approved the submission.

Acknowledgements

Not applicable

Reference

1. Smyth EC, Nilsson M, Grabsch HI, van Grieken NC, Lordick F. Gastric cancer. Lancet. 2020;396(10251):635-48.

2. Chia NY, Tan P. Molecular classification of gastric cancer. Ann Oncol. 2016;27(5):763-9.

3. Wang Q, Chen C, Ding Q, Zhao Y, Wang Z, Chen J, et al. METTL3-mediated m(6)A modification of HDGF mRNA promotes gastric cancer progression and has prognostic significance. Gut. 2020;69(7):1193-205.

4. Yue B, Song C, Yang L, Cui R, Cheng X, Zhang Z, et al. METTL3-mediated N6-methyladenosine modification is critical for epithelial-mesenchymal transition and metastasis of gastric cancer. Mol Cancer. 2019;18(1):142.

5. Roundtree IA, Evans ME, Pan T, He C. Dynamic RNA Modifications in Gene Expression Regulation. Cell. 2017;169(7):1187-200.

6. Cai X, Wang X, Cao C, Gao Y, Zhang S, Yang Z, et al. HBXIP-elevated methyltransferase METTL3 promotes the progression of breast cancer via inhibiting tumor suppressor let-7g. Cancer Lett. 2018;415:11-9.

7. Ma S, Chen C, Ji X, Liu J, Zhou Q, Wang G, et al. The interplay between m6A RNA methylation and noncoding RNA in cancer. J Hematol Oncol. 2019;12(1):121.

8. Chen Y, Lin Y, Shu Y, He J, Gao W. Interaction between N(6)-methyladenosine (m(6)A) modification and noncoding RNAs in cancer. Mol Cancer. 2020;19(1):94.

9. Zheng ZQ, Li ZX, Zhou GQ, Lin L, Zhang LL, Lv JW, et al. Long Noncoding RNA FAM225A Promotes Nasopharyngeal Carcinoma Tumorigenesis and Metastasis by Acting as ceRNA to Sponge miR-590-3p/miR-1275 and Upregulate ITGB3. Cancer Res.

2019;79(18):4612-26.

10. Lan T, Li H, Zhang D, Xu L, Liu H, Hao X, et al. KIAA1429 contributes to liver cancer progression through N6-methyladenosine-dependent post-transcriptional modification of GATA3. Mol Cancer. 2019;18(1):186.

11. Yan J, Huang X, Zhang X, Chen Z, Ye C, Xiang W, et al. LncRNA LINC00470 promotes the degradation of PTEN mRNA to facilitate malignant behavior in gastric cancer cells. Biochem Biophys Res Commun. 2020;521(4):887-93.

12. Hinshaw DC, Shevde LA. The Tumor Microenvironment Innately Modulates Cancer Progression. Cancer Res. 2019;79(18):4557-66.

13. Zhang B, Wu Q, Li B, Wang D, Wang L, Zhou YL. m(6)A regulator-mediated methylation modification patterns and tumor microenvironment infiltration characterization in gastric cancer. Mol Cancer. 2020;19(1):53.

14. Chong W, Shang L, Liu J, Fang Z, Du F, Wu H, et al. m(6)A regulator-based methylation modification patterns characterized by distinct tumor microenvironment immune profiles in colon cancer. Theranostics. 2021;11(5):2201-17.

15. Yi L, Wu G, Guo L, Zou X, Huang P. Comprehensive Analysis of the PD-L1 and Immune Infiltrates of m(6)A RNA Methylation Regulators in Head and Neck Squamous Cell Carcinoma. Mol Ther Nucleic Acids. 2020;21:299-314.

16. Tu Z, Wu L, Wang P, Hu Q, Tao C, Li K, et al. N6-Methylandenosine-Related lncRNAs Are Potential Biomarkers for Predicting the Overall Survival of Lower-Grade Glioma Patients. Front Cell Dev Biol. 2020;8:642.

17. Yi YC, Chen XY, Zhang J, Zhu JS. Novel insights into the interplay between m(6)A

modification and noncoding RNAs in cancer. Mol Cancer. 2020;19(1):121.

18. Zhou KI, Parisien M, Dai Q, Liu N, Diatchenko L, Sachleben JR, et al. N(6)-Methyladenosine Modification in a Long Noncoding RNA Hairpin Predisposes Its Conformation to Protein Binding. J Mol Biol. 2016;428(5 Pt A):822-33.

19. Zuo X, Chen Z, Gao W, Zhang Y, Wang J, Wang J, et al. M6A-mediated upregulation of LINC00958 increases lipogenesis and acts as a nanotherapeutic target in hepatocellular carcinoma. J Hematol Oncol. 2020;13(1):5.

20. Zhang S, Zhao BS, Zhou A, Lin K, Zheng S, Lu Z, et al. m(6)A Demethylase ALKBH5 Maintains Tumorigenicity of Glioblastoma Stem-like Cells by Sustaining FOXM1 Expression and Cell Proliferation Program. Cancer Cell. 2017;31(4):591-606.e6.

21. Wang X, Zhang J, Wang Y. Long noncoding RNA GAS5-AS1 suppresses growth and metastasis of cervical cancer by increasing GAS5 stability. Am J Transl Res. 2019;11(8):4909-21.

22. Han D, Liu J, Chen C, Dong L, Liu Y, Chang R, et al. Anti-tumour immunity controlled through mRNA m(6)A methylation and YTHDF1 in dendritic cells. Nature. 2019;566(7743):270-4.

23. Wang L, Hui H, Agrawal K, Kang Y, Li N, Tang R, et al. m(6) A RNA methyltransferases METTL3/14 regulate immune responses to anti-PD-1 therapy. Embo j. 2020;39(20):e104514.

24. Chen YG, Satpathy AT, Chang HY. Gene regulation in the immune system by long noncoding RNAs. Nat Immunol. 2017;18(9):962-72.

25. Wang CJ, Zhu CC, Xu J, Wang M, Zhao WY, Liu Q, et al. The lncRNA UCA1 promotes proliferation, migration, immune escape and inhibits apoptosis in gastric cancer by sponging anti-tumor miRNAs. Mol Cancer. 2019;18(1):115.

26. Gomez JA, Wapinski OL, Yang YW, Bureau JF, Gopinath S, Monack DM, et al. The NeST long ncRNA controls microbial susceptibility and epigenetic activation of the interferon-γ locus. Cell. 2013;152(4):743-54.

27. Sehgal L, Mathur R, Braun FK, Wise JF, Berkova Z, Neelapu S, et al. FAS-antisense 1 lncRNA and production of soluble versus membrane Fas in B-cell lymphoma. Leukemia. 2014;28(12):2376-87.

28. Li Y, Jiang T, Zhou W, Li J, Li X, Wang Q, et al. Pan-cancer characterization of immune-related lncRNAs identifies potential oncogenic biomarkers. Nat Commun. 2020;11(1):1000.

29. Galluzzi L, Humeau J, Buqué A, Zitvogel L, Kroemer G. Immunostimulation with chemotherapy in the era of immune checkpoint inhibitors. Nat Rev Clin Oncol. 2020;17(12):725-41.

30. Chen C, Zhang F, Zhou N, Gu YM, Zhang YT, He YD, et al. Efficacy and safety of immune checkpoint inhibitors in advanced gastric or gastroesophageal junction cancer: a systematic review and meta-analysis. Oncoimmunology. 2019;8(5):e1581547.

31. Lazăr DC, Avram MF, Romoșan I, Cornianu M, Tăban S, Goldiș A. Prognostic significance of tumor immune microenvironment and immunotherapy: Novel insights and future perspectives in gastric cancer. World J Gastroenterol. 2018;24(32):3583-616.

32. Gajewski TF, Schreiber H, Fu YX. Innate and adaptive immune cells in the tumor microenvironment. Nat Immunol. 2013;14(10):1014-22.

33. Song WM, Lin X, Liao X, Hu D, Lin J, Sarpel U, et al. Multiscale network analysis reveals molecular mechanisms and key regulators of the tumor microenvironment in gastric cancer. Int J

Cancer. 2020;146(5):1268-80.

34. Coutzac C, Pernot S, Chaput N, Zaanan A. Immunotherapy in advanced gastric cancer, is it the future? Crit Rev Oncol Hematol. 2019;133:25-32.

35. Patel S, Alam A, Pant R, Chattopadhyay S. Wnt Signaling and Its Significance Within the Tumor Microenvironment: Novel Therapeutic Insights. Front Immunol. 2019;10:2872.

36. Crotty S. T Follicular Helper Cell Biology: A Decade of Discovery and Diseases. Immunity. 2019;50(5):1132-48.

37. Marrelli D, Polom K, Pascale V, Vindigni C, Piagnerelli R, De Franco L, et al. Strong Prognostic Value of Microsatellite Instability in Intestinal Type Non-cardia Gastric Cancer. Ann Surg Oncol. 2016;23(3):943-50.

38. Shitara K, Özgüroğlu M, Bang YJ, Di Bartolomeo M, Mandalà M, Ryu MH, et al. Pembrolizumab versus paclitaxel for previously treated, advanced gastric or gastro-oesophageal junction cancer (KEYNOTE-061): a randomised, open-label, controlled, phase 3 trial. Lancet. 2018;392(10142):123-33.

39. Fuchs CS, Doi T, Jang RW, Muro K, Satoh T, Machado M, et al. Safety and Efficacy of Pembrolizumab Monotherapy in Patients With Previously Treated Advanced Gastric and Gastroesophageal Junction Cancer: Phase 2 Clinical KEYNOTE-059 Trial. JAMA Oncol. 2018;4(5):e180013.

40. Chalmers ZR, Connelly CF, Fabrizio D, Gay L, Ali SM, Ennis R, et al. Analysis of 100,000 human cancer genomes reveals the landscape of tumor mutational burden. Genome Med. 2017;9(1):34.

Figure legends

Figure 1

Study flow chart of this study.

Figure 2

The lncRNAs significantly correlated with m6A-related genes. (A) Co-expression network of m6A-related genes and lncRNAs. (B) Forest plot of the prognostic ability of the 23 m6A-related lncRNAs. (C, D) Heatmap (C) and expression value (D) of the 23 m6A-related lncRNAs in 32 normal tissues and 375 tumor tissues. * $p<0.05$, ** $p<0.01$, *** $p<0.001$.

Figure 3

Differential survival outcome of GC in cluster 1/2 subtypes. (A) Consensus score matrix of all samples when k=3. (B) The cumulative distribution functions (CDF) for k=2 to 9. (C) Relative change in area under CDF area for k=2 to 9. (D-I) Survival analysis of cluster 1/2 subtypes in the total TCGA cohort (D) and samples of age less than or equal to 65 (E), female (F), male (G), grade 3 (H) and stage III-IV (I).

Figure 4

ESTIMATE analysis and GESA in cluster 1/2 subtypes. (A-C) comparison of immune score (A), stromal score (B) and ESTIMATE score (C) in two subtypes. (D-F) GSEA showed that cell adhesion molecules, ECM receptor interaction and focal adhesion are differentially enriched in cluster1. NES, normalized enrichment score; NOM p-val, normalized p value; FDR q value: false discovery rate q value

Figure 5

Comparison of immune cells infiltration between cluster 1/2 subtypes. (A-F) The infiltrating

levels of CD4 memory activated T cells (A), CD4 memory resting T cells (B), follicular helper T cells (C), monocytes (D), macrophages M1 (E) and resting mast cells (F) in two subtypes. (G) The fraction of 22 types of infiltrating immune cells in cluster 1/2 subtypes.

Figure 6

Frequently mutated genes in cluster 1/2 subtypes. (A, B) Waterfall plots display the frequently mutated genes in 2 clusters of gastric cancer. The left panel shows the genes ordered by their mutation frequencies. The right panel shows different mutation types.

Figure 7

Construction of the GC prognostic risk model based on 9 m6A-related lncRNAs. (A, B) Least absolute shrinkage and selection operator (LASSO) regression was performed, the penalization coefficient λ in the LASSO model was tuned using 10-fold cross-validation and minimum criterion for the selection of m6A-related lncRNAs. (C) Barplot of the coefficients of selected lncRNAs. (D, E) kaplan-Meier analysis showed that high risk group exhibited worse survival outcome than the low risk group in the training (D) and validation (E) cohort. (F, G) Receiver operating characteristic (ROC) curves of risk model for predicting survival in the training (F) and validation cohort (G). (H, I) Distribution of risk score, survival status of GC patients and heatmap of the 9 m6A-related lncRNAs in high/low risk group in the training (H) and validation (I) cohort.

Figure 8

Prognostic risk score correlated with clinicopathological features and cluster1/2 subtypes. (A) Heatmap of clinicopathological features, immune score and different lncRNAs expression pattern in high/low risk group. (B-E) Comparison of risk score distribution in the different sample classification of cluster1/2 (B), grade1-2/grade3 (C), stage I-II/III-IV (D)and N0/N1-3 (E). *

$p<0.05$, ** $p<0.01$, *** $p<0.001$.

Figure 9

Relationships between risk score and infiltration level of six immune cell types. (A) CD4 memory activated T cells, (B) macrophages M0, (C) macrophages M2, (D) follicular helper T cells, (E) resting dendritic cells and (F) memory B cells.

Figure 10

The associations between risk score and tumor mutational burden, microsatellite status and immunotherapy gene expression. (A) The expression levels of tumor mutation burden in low and high risk group. (B) The correlation of risk score and tumor mutation burden. (C) The distribution of microsatellite status in different risk group. (D) The risk score in patients with different microsatellite status. (E-H) The gene expression pattern of PD1 and CTLA4 in high risk and low risk groups.

Figure 11

External validation the expression levels of these 9 m6A-related lncRNAs and their prognostic value in 35 GC patients. (A) The heatmap showed the expression pattern of 9 m6A-related lncRNAs in 35 GC tissues and adjacent normal tissues. (B) Survival analysis of 35 GC patients in different risk groups. (C) Receiver operating characteristic (ROC) curves of risk model for predicting survival in 35 GC patients. (D) Time dependent AUC analysis where the solid and dashed lines depict the AUC and its 95% CI respectively. (E) The calibration curves of risk score for the prediction of survival.

Figures

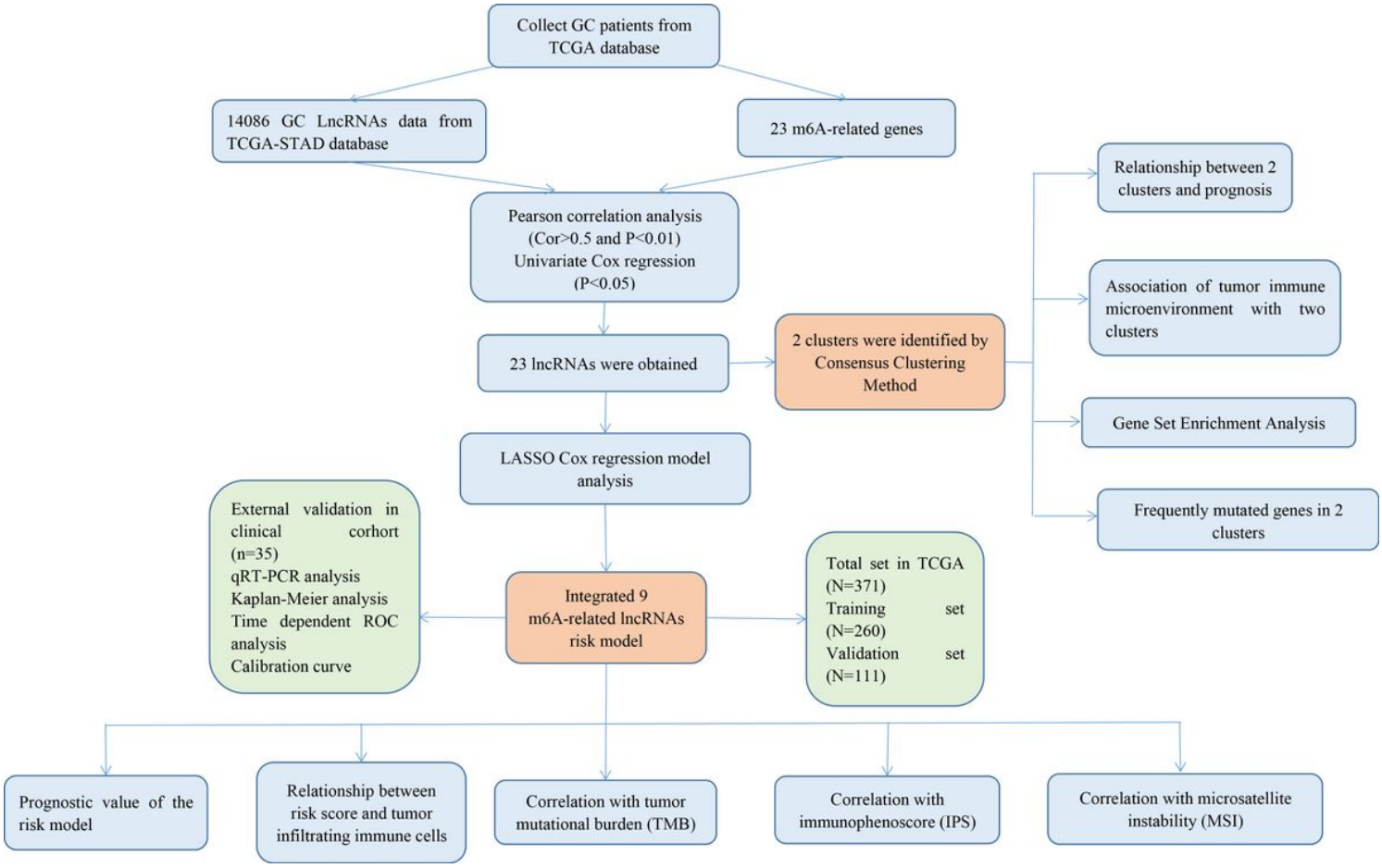

Figure 1

Study flow chart of this study.

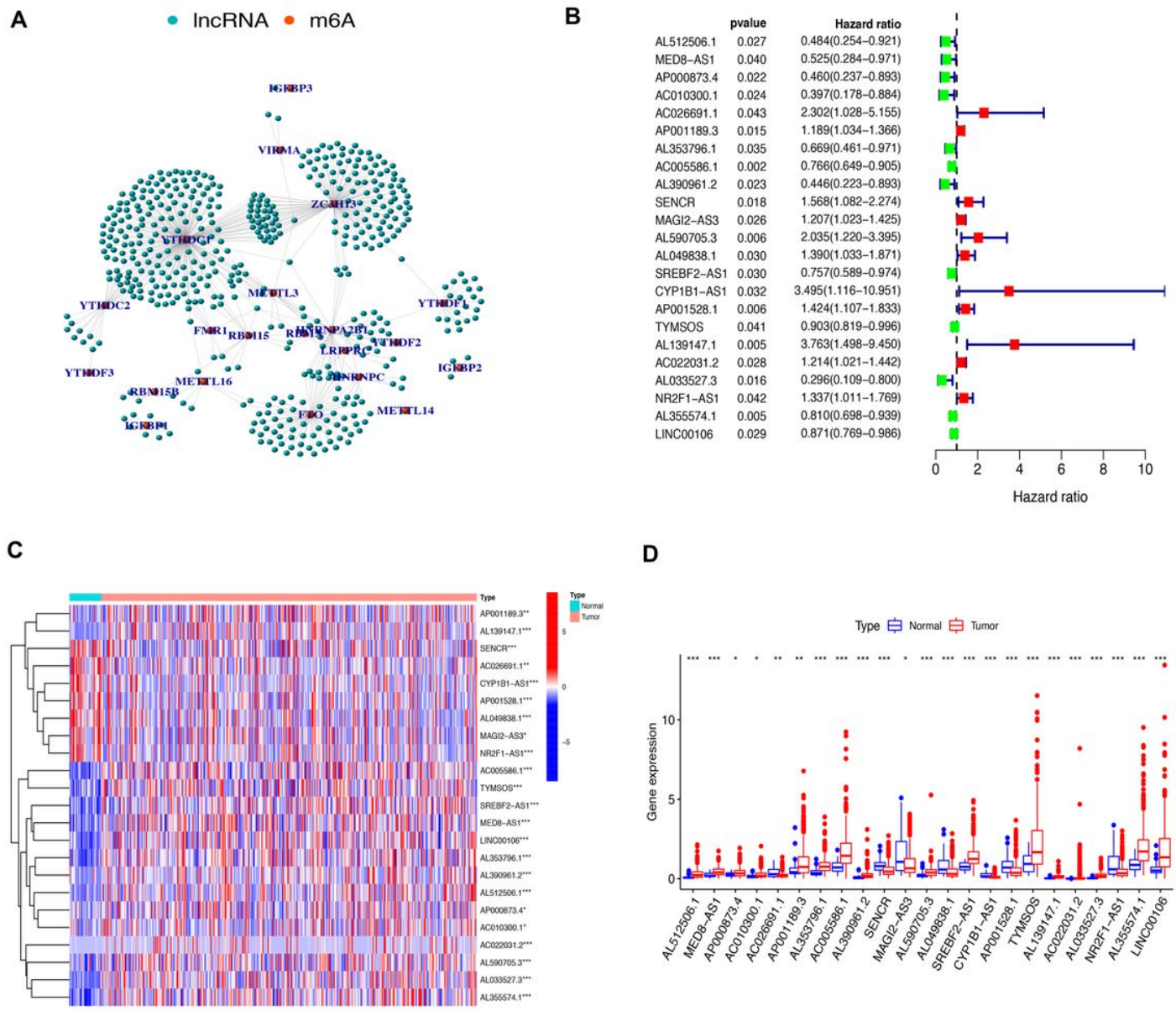

Figure 2

The lncRNAs significantly correlated with m6A-related genes. (A) Co-expression network of m6A-related genes and lncRNAs. (B) Forest plot of the prognostic ability of the 23 m6A-related lncRNAs. (C, D) Heatmap (C) and expression value (D) of the 23 m6A-related lncRNAs in 32 normal tissues and 375 tumor tissues. * p<0.05, ** p<0.01, *** p<0.001.

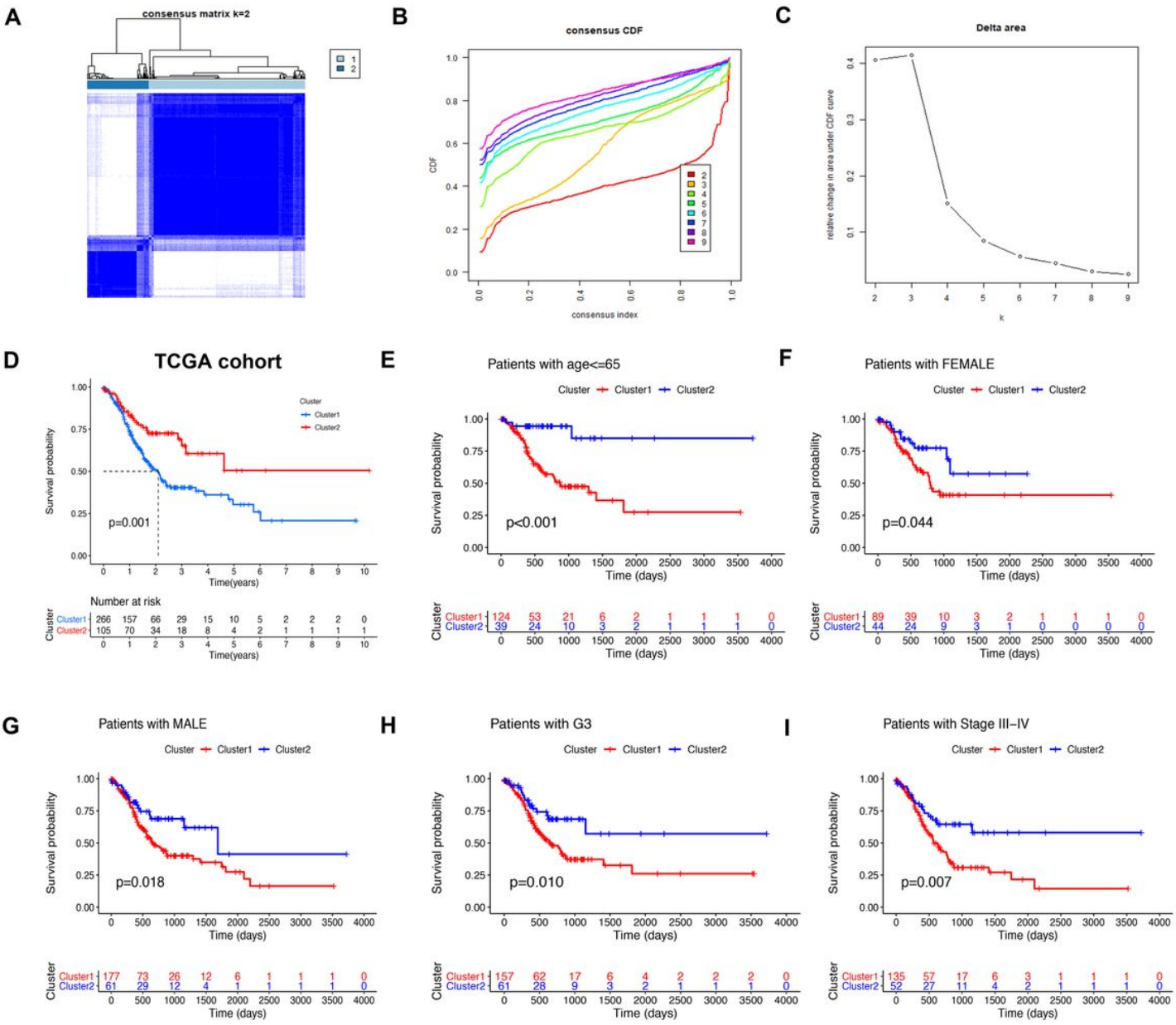

Figure 3

Differential survival outcome of GC in cluster 1/2 subtypes. (A) Consensus score matrix of all samples when k=3. (B) The cumulative distribution functions (CDF) for k=2 to 9. (C) Relative change in area under CDF area for k=2 to 9. (D-I) Survival analysis of cluster 1/2 subtypes in the total TCGA cohort (D) and samples of age less than or equal to 65 (E), female (F), male (G), grade 3 (H) and stage III-IV (I).

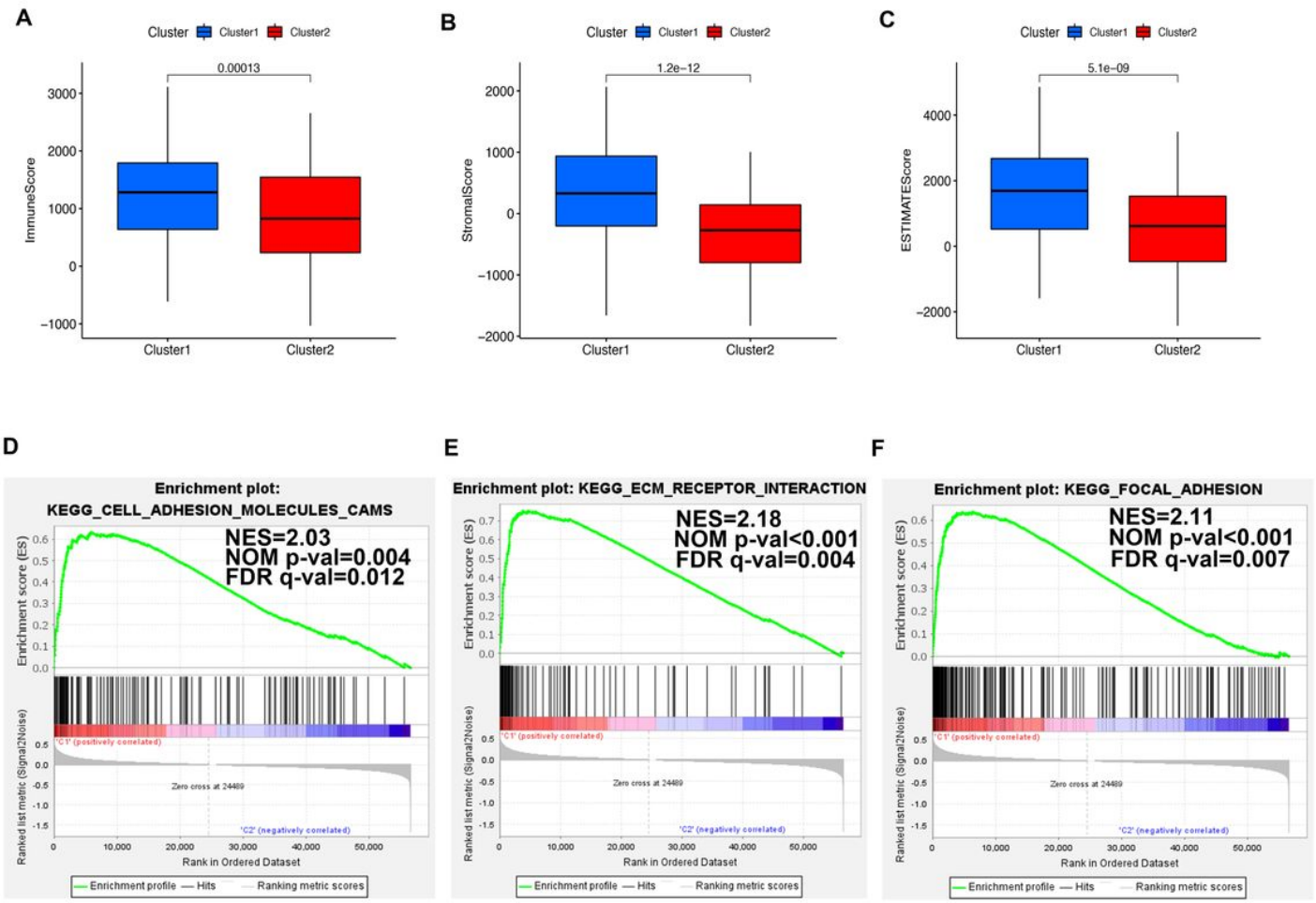

Figure 4

ESTIMATE analysis and GESA in cluster 1/2 subtypes. (A-C) comparison of immune score (A), stromal score (B) and ESTIMATE score (C) in two subtypes. (D-F) GSEA showed that cell adhesion molecules, ECM receptor interaction and focal adhesion are differentially enriched in cluster1. NES, normalized enrichment score; NOM p-val, normalized p value; FDR q value: false discovery rate q value

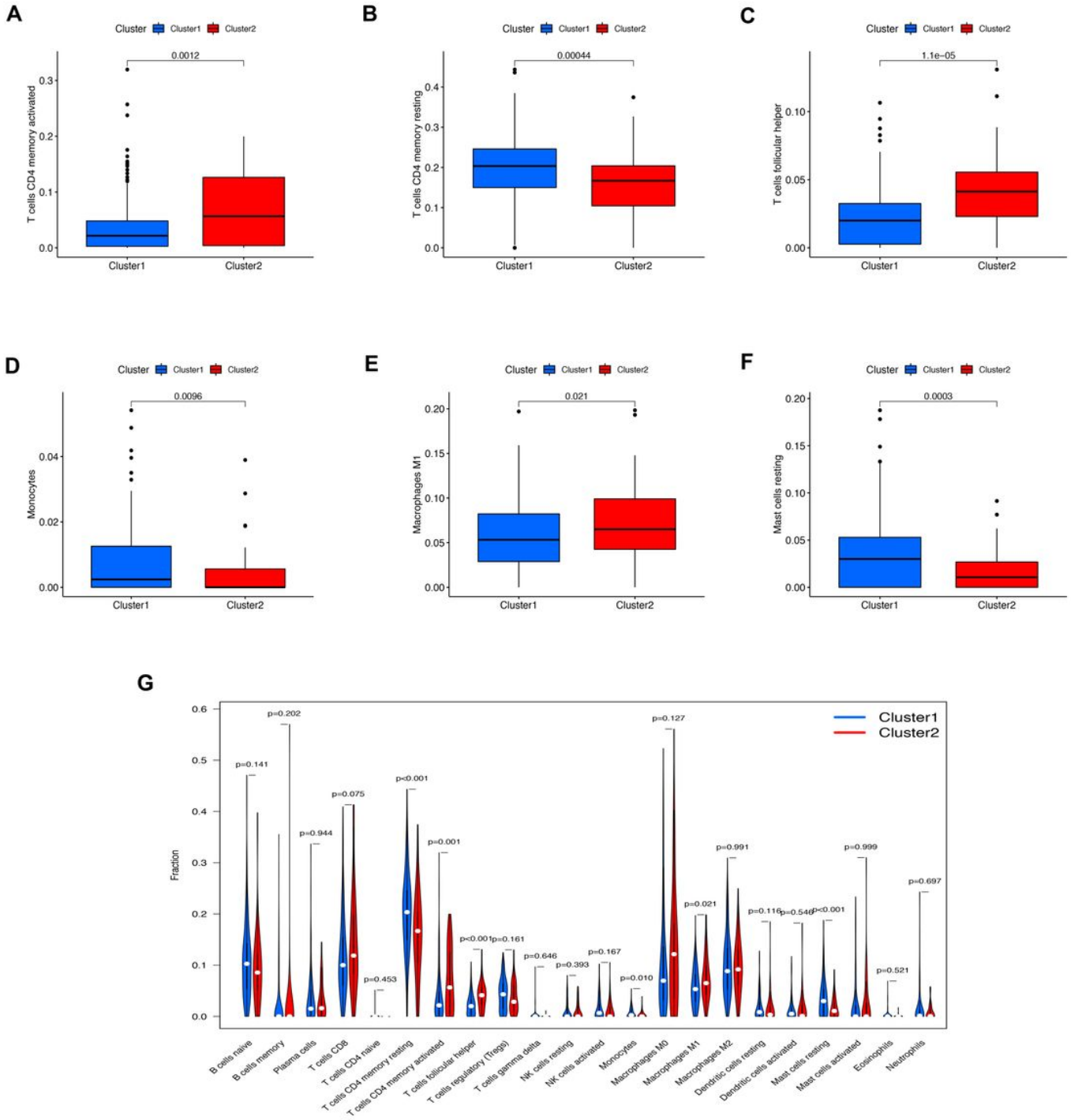

Figure 5

Comparison of immune cells infiltration between cluster 1/2 subtypes. (A-F) The infiltrating levels of CD4 memory activated T cells (A), CD4 memory resting T cells (B), follicular helper T cells (C), monocytes (D), macrophages M1 (E) and resting mast cells (F) in two subtypes. (G) The fraction of 22 types of infiltrating immune cells in cluster 1/2 subtypes.

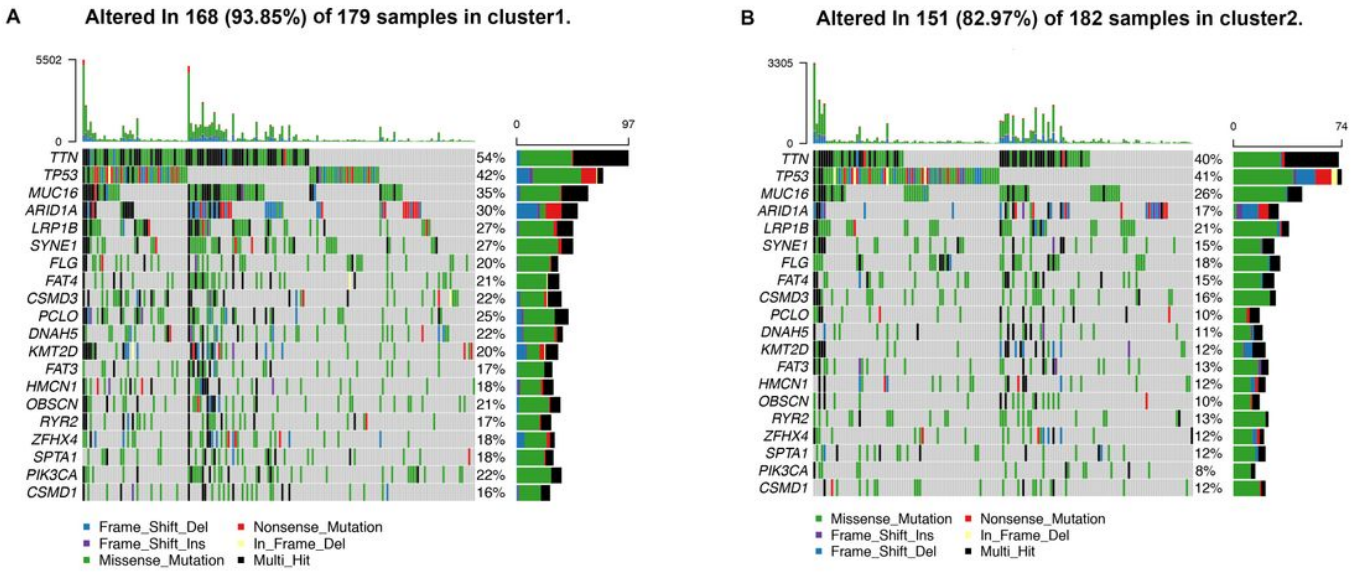

Figure 6

Frequently mutated genes in cluster 1/2 subtypes. (A, B) Waterfall plots display the frequently mutated genes in 2 clusters of gastric cancer. The left panel shows the genes ordered by their mutation frequencies. The right panel shows different mutation types.

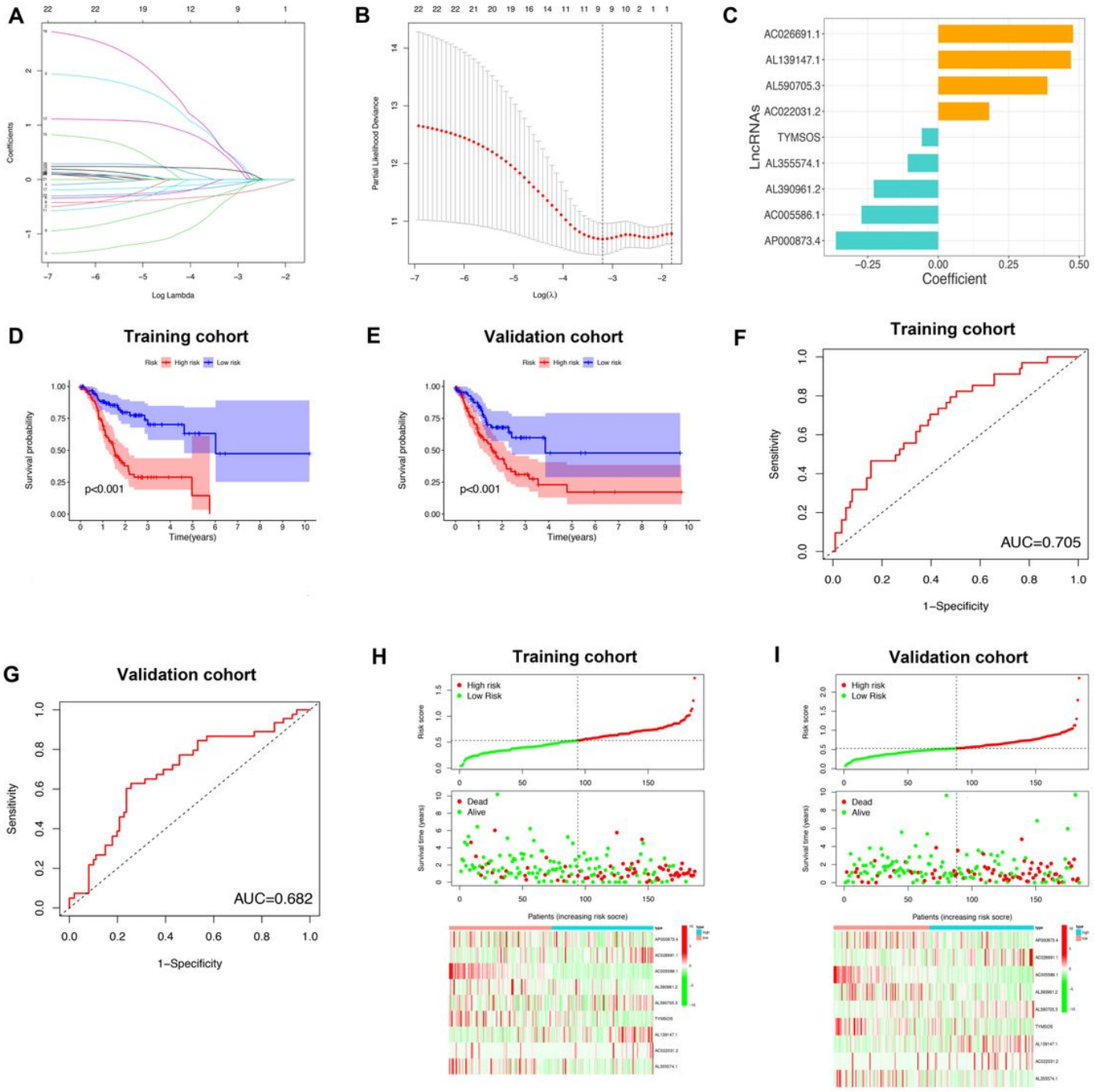

Figure 7

Construction of the GC prognostic risk model based on 9 m6A-related lncRNAs. (A, B) Least absolute shrinkage and selection operator (LASSO) regression was performed, the penalization coefficient λ in the LASSO model was tuned using 10-fold cross-validation and minimum criterion for the selection of m6A-related lncRNAs. (C) Barplot of the coefficients of selected lncRNAs. (D, E) kaplan-Meier analysis showed that high risk group exhibited worse survival outcome than the low risk group in the training (D) and validation (E) cohort. (F, G) Receiver operating characteristic (ROC) curves of risk model for predicting

survival in the training (F) and validation cohort (G). (H, I) Distribution of risk score, survival status of GC patients and heatmap of the 9 m6A-related lncRNAs in high/low risk group in the training (H) and validation (I) cohort.

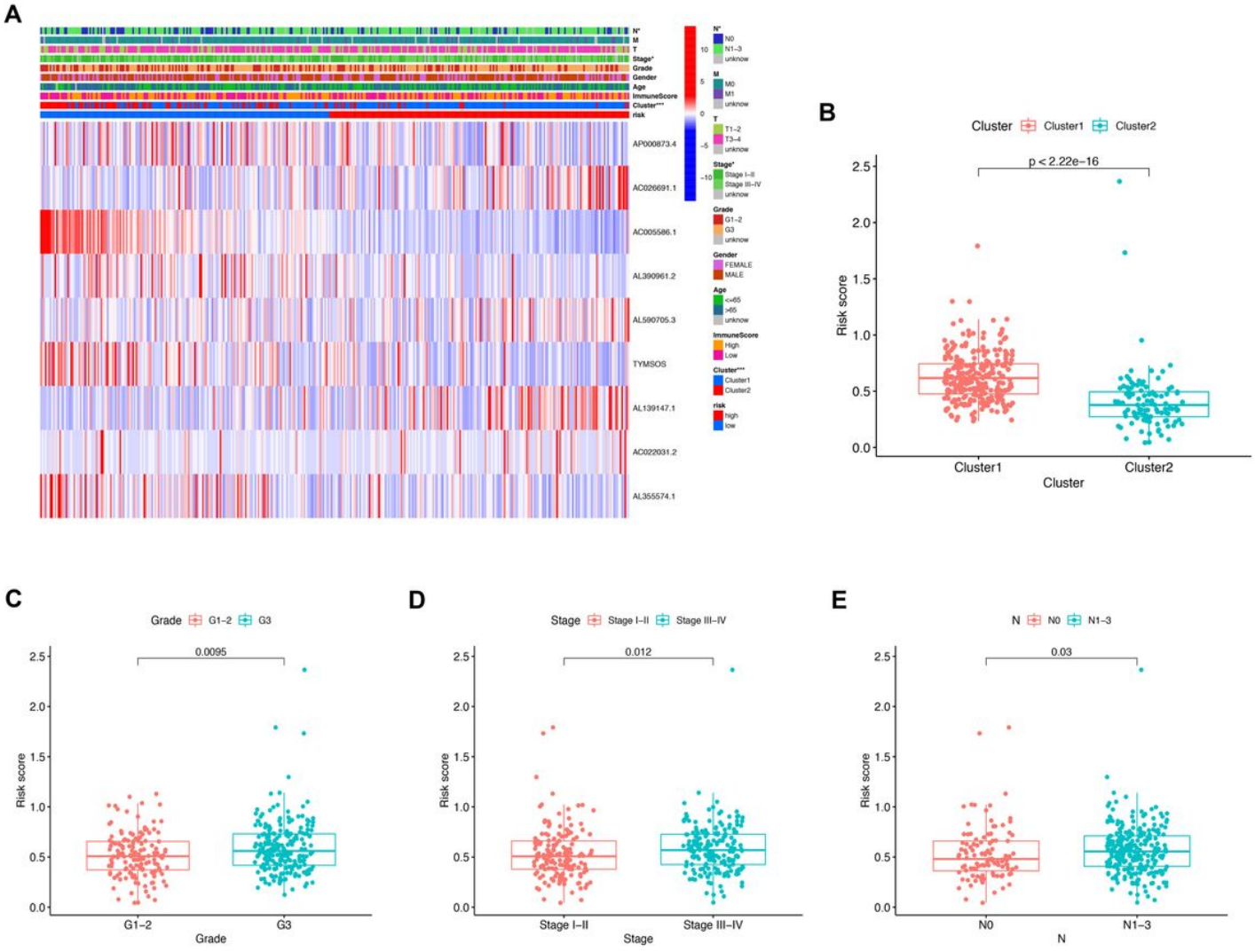

Figure 8

Prognostic risk score correlated with clinicopathological features and cluster1/2 subtypes. (A) Heatmap of clinicopathological features, immune score and different lncRNAs expression pattern in high/low risk group. (B-E) Comparison of risk score distribution in the different sample classification of cluster1/2 (B), grade1-2/grade3 (C), stage I-II/III-IV (D)and N0/N1-3 (E). * p<0.05, ** p<0.01, *** p<0.001.

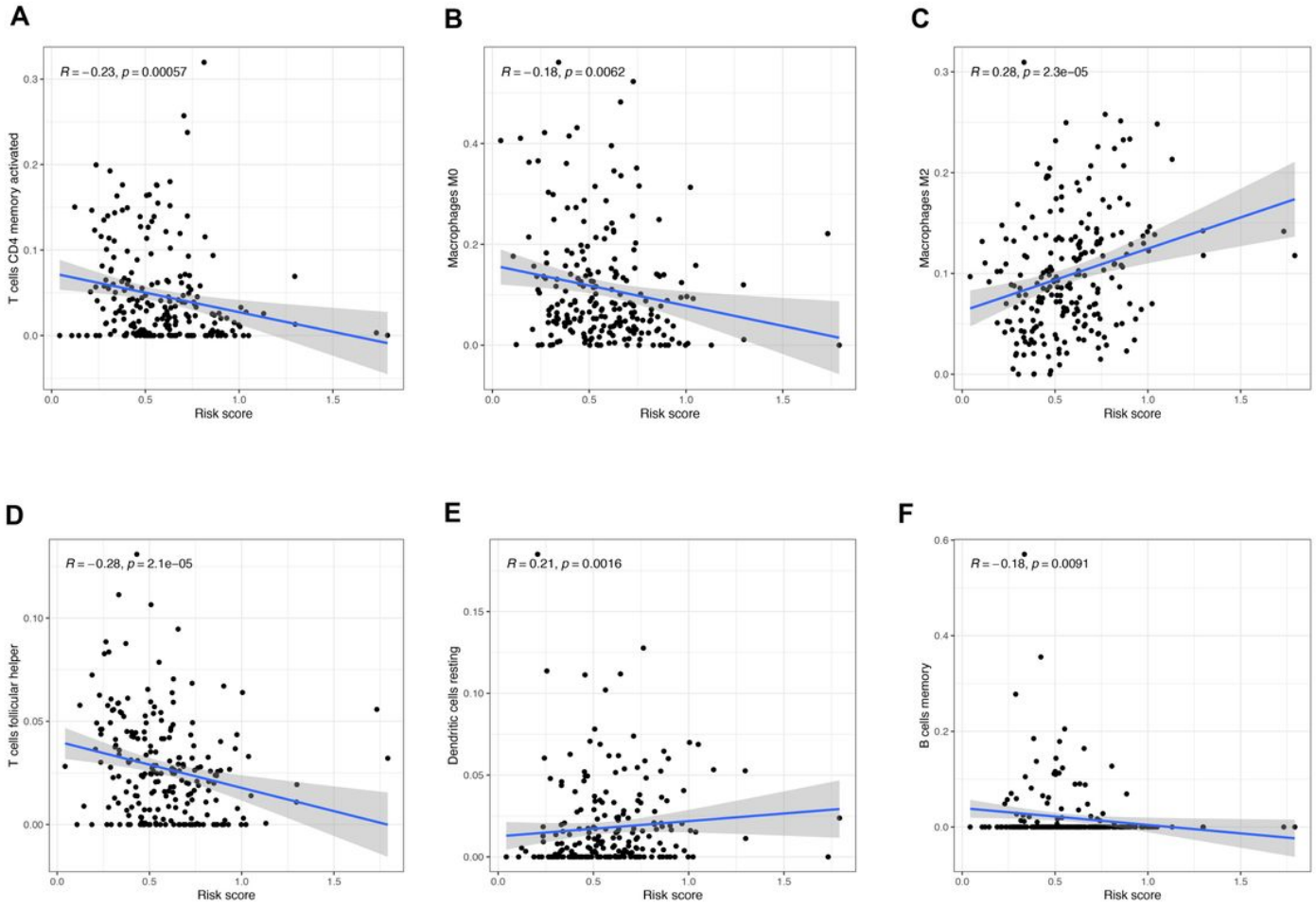

Figure 9

Relationships between risk score and infiltration level of six immune cell types. (A) CD4 memory activated T cells, (B) macrophages M0, (C) macrophages M2, (D) follicular helper T cells, (E) resting dendritic cells and (F) memory B cells.

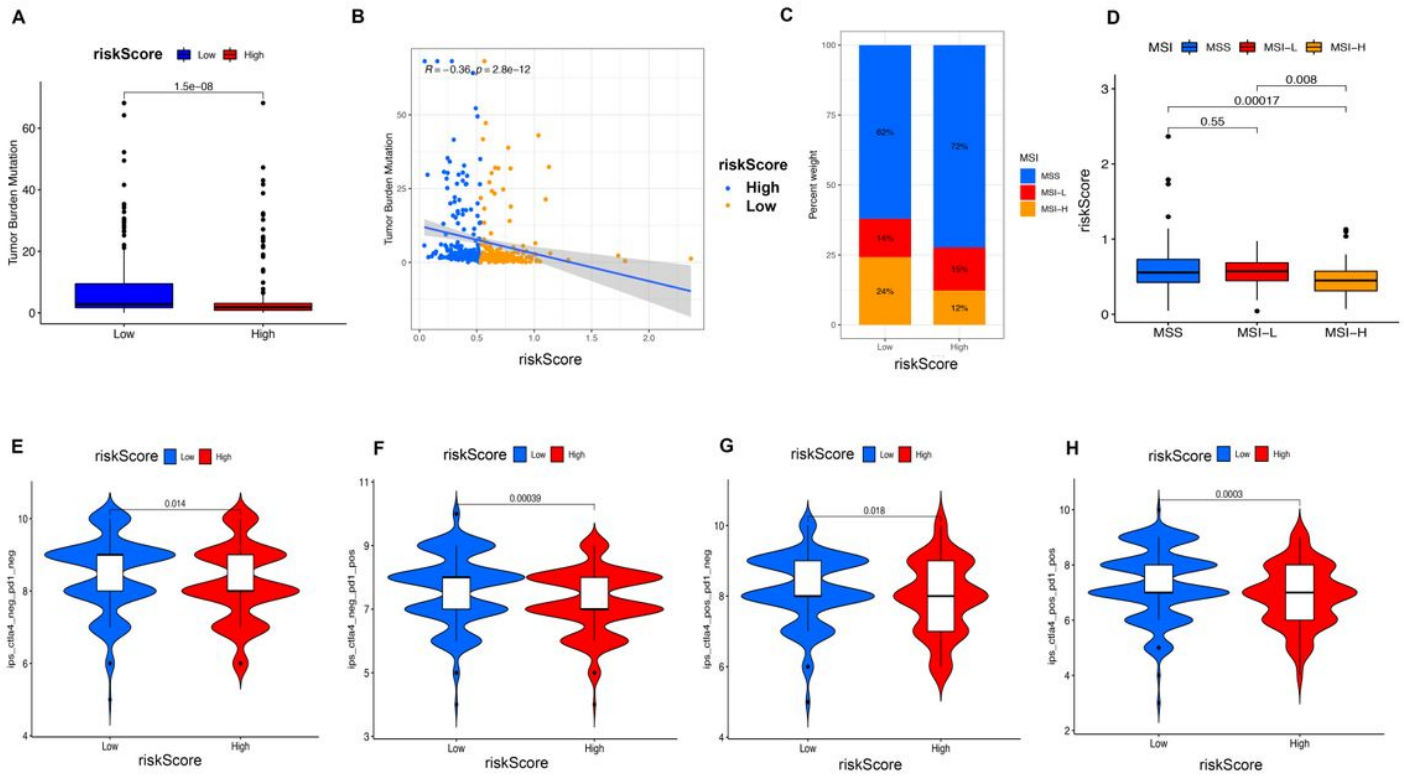

Figure 10

The associations between risk score and tumor mutational burden, microsatellite status and immunotherapy gene expression. (A) The expression levels of tumor mutation burden in low and high risk group. (B) The correlation of risk score and tumor mutation burden. (C) The distribution of microsatellite status in different risk group. (D) The risk score in patients with different microsatellite status. (E-H) The gene expression pattern of PD1 and CTLA4 in high risk and low risk groups.

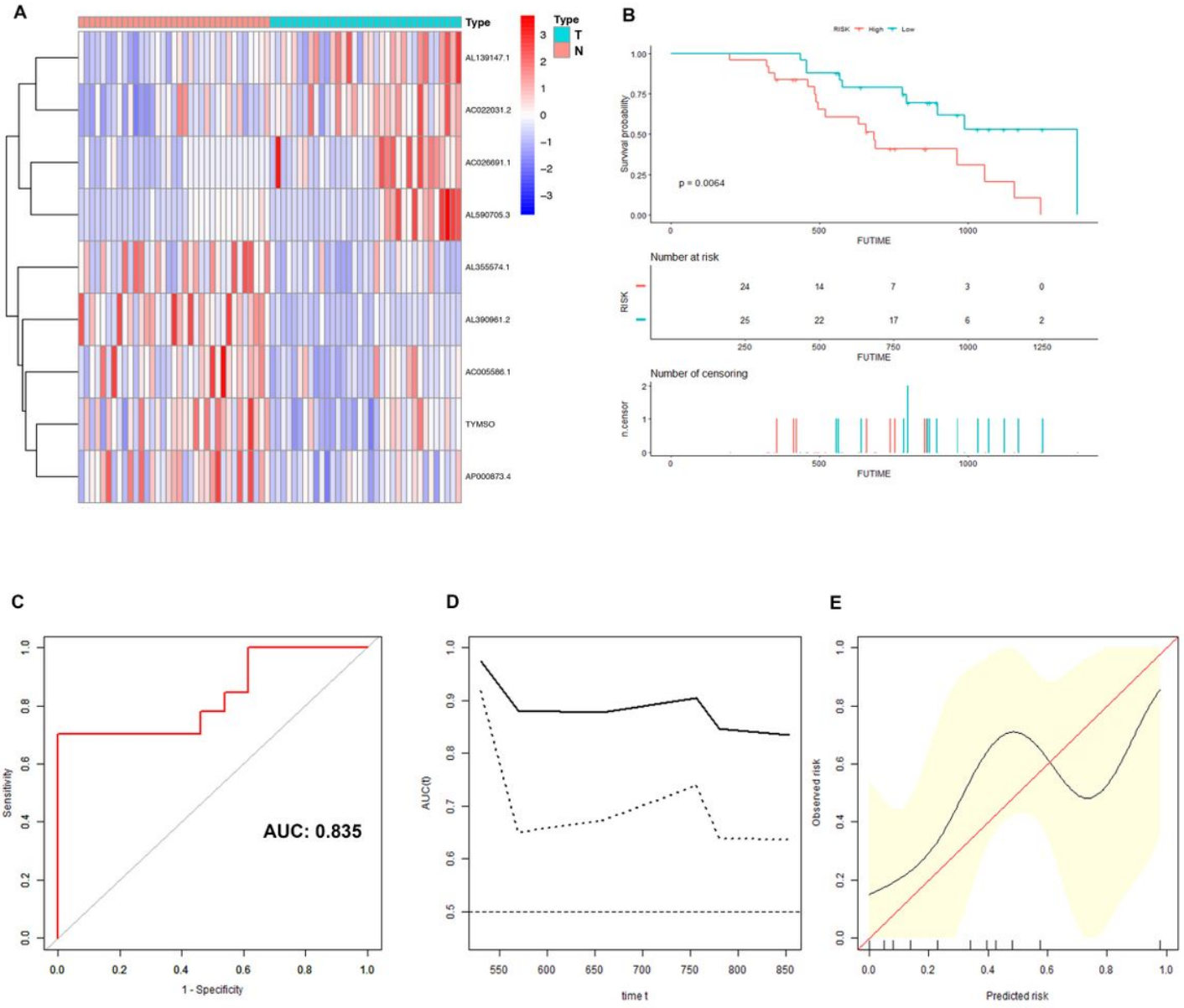

Figure 11

External validation the expression levels of these 9 m6A-related lncRNAs and their prognostic value in 35 GC patients. (A) The heatmap showed the expression pattern of 9 m6A-related lncRNAs in 35 GC tissues and adjacent normal tissues. (B) Survival analysis of 35 GC patients in different risk groups. (C) Receiver operating characteristic (ROC) curves of risk model for predicting survival in 35 GC patients. (D) Time dependent AUC analysis where the solid and dashed lines depict the AUC and its 95% CI respectively. (E) The calibration curves of risk score for the prediction of survival.

Supplementary Files

This is a list of supplementary files associated with this preprint. Click to download.

- Supplementarymaterials.docx